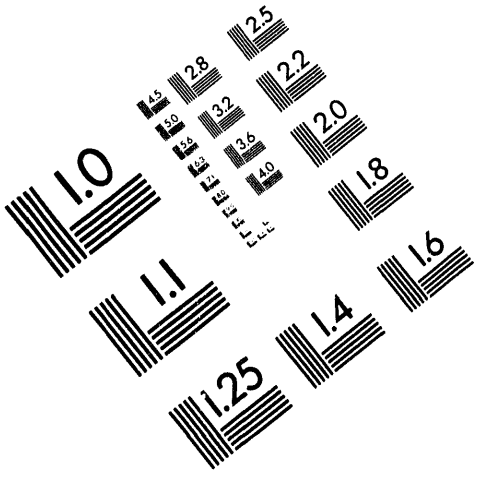

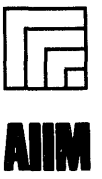

Association for Information and Image Management
1100 Wayne Avenue, Suite 1100
Silver Spring, Maryland 20910
301/587-8202

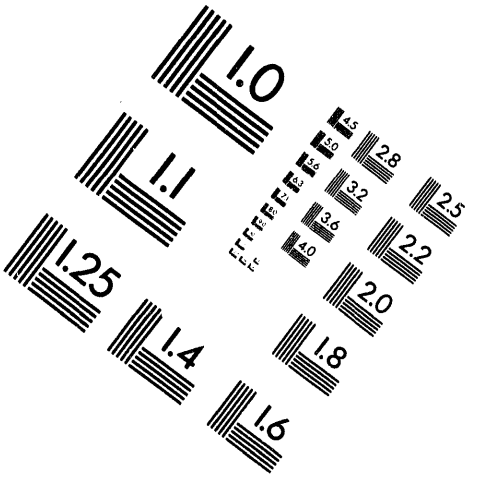

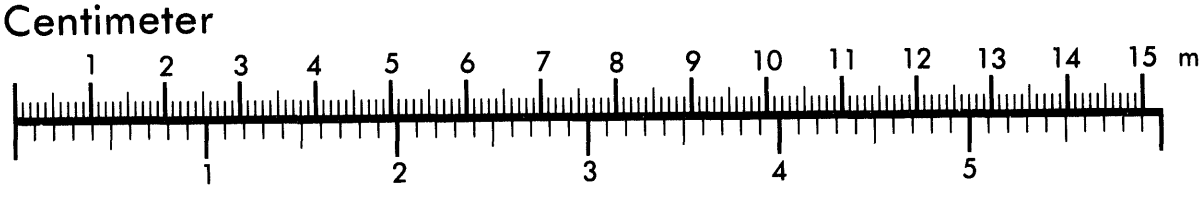

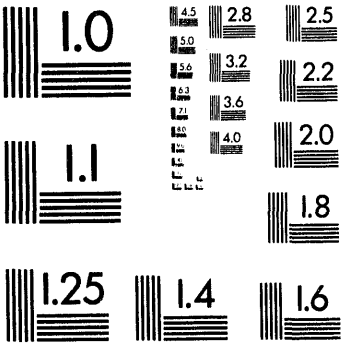

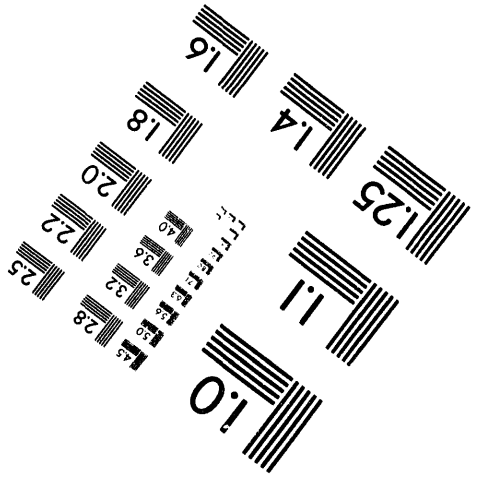

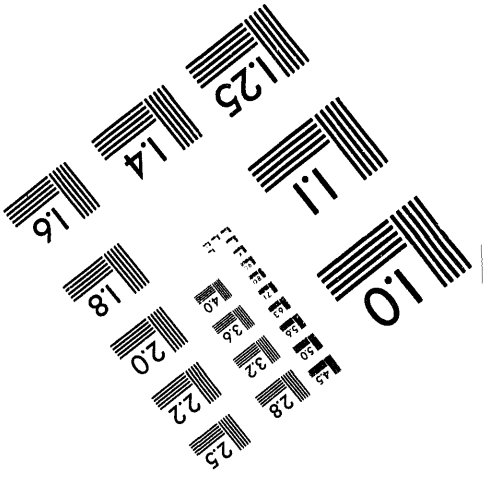

MANUFACTURED TO AIIM STANDARDS
BY APPLIED IMAGE, INC.

1 of 1

Conf-940391--11

UCRL-JC-115104
PREPRINT

Simulation of Stellar Speckle Imaging

E. M. Johansson
D. T. Gavel
Lawrence Livermore National Laboratory

This paper was prepared for submission to
SPIE's Symposium on Astronomical Telescopes and Instrumentation
for the 21st Century, March 13-18, 1994
Kona, Hawaii

April 1994

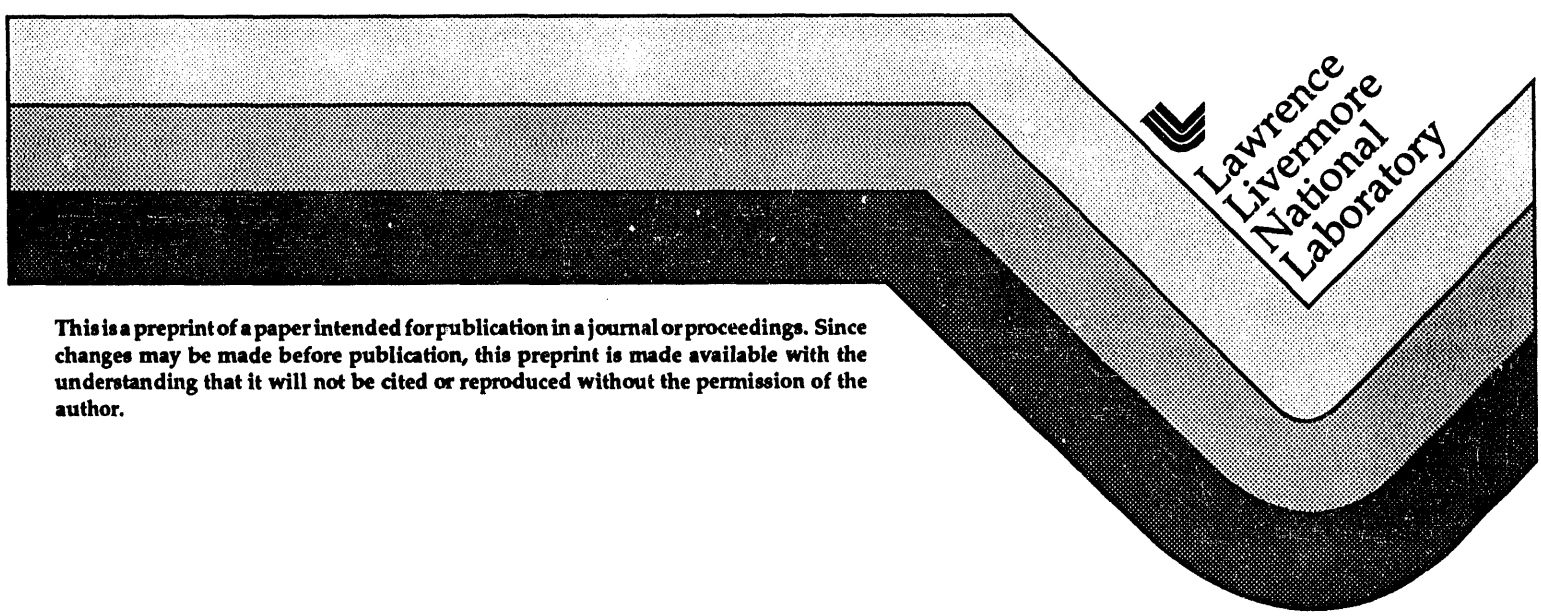

Simulation of stellar speckle imaging

E. M. Johansson and D. T. Gavel

University of California, Lawrence Livermore National Laboratory
PO Box 808, L-495, Livermore, CA 94550

ABSTRACT

Standard FFT-based phase screen generation methods do not accurately model low frequency turbulence characteristics. This paper introduces a new phase screen generation technique which uses low frequency subharmonic information to correct the problem. We compare our technique to two other subharmonic methods. The structure functions for this new method match very closely the structure functions of Kolmogorov turbulence theory.

1 INTRODUCTION

Simulation of the wavefront distortions caused by atmospheric turbulence has long been an important tool in the study of the propagation of light through the atmosphere, in the design of large astronomical telescopes and adaptive optics systems, and in the development of advanced speckle imaging algorithms. The effects of the turbulent atmosphere are usually simulated using thin phase screens which perturb the phase of a propagating wavefront in accordance with Kolmogorov theory. Although there are several techniques for generating phase screens (e.g., the Zernike method of Roddier [1] and the random mid-point displacement method of Lane, et al. [2]), the most popular methods are based on filtering white Gaussian noise in the spectral domain (wavenumber space) and then transforming to the spatial domain using the fast Fourier transform (FFT) [3, 4, 5]. These FFT-based techniques are limited in that they do not accurately reproduce the low spatial frequency characteristics of Kolmogorov turbulence. Several researchers have investigated extending these techniques to incorporate low frequency information [2, 6]. In this paper we develop a new low frequency simulation technique, which is a hybrid version of these previous methods, specifically for the purpose of generating very long narrow phase screens to be used in time varying turbulence simulations.

This paper is organized as follows: we begin with a brief review of the atmospheric turbulence theory required to generate phase screens. We then review the FFT-based method of phase screen generation, show why it is inaccurate, and discuss how to solve the problem using subharmonic information. Next, we discuss two current subharmonic methods and how their results compare to theory. Finally we introduce a new subharmonic method which has excellent results which agree closely with theory.

2 REVIEW OF ATMOSPHERIC TURBULENCE THEORY

The statistical nature of the turbulence-induced fluctuations in the refractive index of the atmosphere has been well characterized (see [7] and [8] for good tutorial introductions). Hence, we include only the details necessary for an understanding of the generation of phase screens. Our summary discussion is a compilation of the theory presented in several sources [6, 7, 8, 9].

We begin by assuming isotropic and homogeneous turbulence, and use the von Kármán model for the power spectral density of the refractive index fluctuations of the atmosphere, which is given by

$$\Phi_n(\kappa, z) = 0.033\, C_n^2(z)(\kappa^2 + \kappa_0^2)^{-11/6} e^{-\kappa^2/\kappa_i^2} \tag{1}$$

where z is the direction of propagation and $C_n^2(z)$ is the structure constant which represents the strength of the turbulence at each position z in the propagation. The variable κ is the three-dimensional (3D) spatial wavenumber

$$\kappa = (\kappa_x^2 + \kappa_y^2 + \kappa_z^2)^{1/2} \tag{2}$$

where $\kappa_x = 2\pi/x$, $\kappa_y = 2\pi/y$, and $\kappa_z = 2\pi/z$ are the individual 1D wavenumbers, and x, y, and z are the associated scale sizes of the turbulence (throughout this paper, we allow the minor abuse of notation that a variable without its corresponding vector arrow denotes the magnitude of the vector). Thus, we see that for $\kappa < \kappa_0$, $\Phi_n(\kappa, z)$ is limited by κ_0, and for $\kappa > \kappa_i$, $\Phi_n(\kappa, z)$ is very quickly forced to zero. These critical wavenumbers correspond to turbulence scale lengths $L_0 = 2\pi/\kappa_0$ and $l_0 = 2\pi/\kappa_i$. L_0 is called the outer scale and l_0 is called the inner scale.

In numerical implementations, κ_i may be ignored, because the ratio of $\Phi_n(\kappa_0, z)/\Phi_n(\kappa_i, z)$ (the dynamic range of the spectrum to be simulated) is several orders of magnitude. For example, assuming $L_0 = 10$ m and $l_0 = 0.01$ m, we calculate $\Phi_n(\kappa_0, z)/\Phi_n(\kappa_i, z) = 10^{11}$. Hence, the dynamic range of the spectrum is so large that in a single precision simulation, the effect of the roll-off due to the presence of κ_i in the model will most likely not be noticed. Therefore, for the purposes of our discussion, we use the following modified von Kármán spectrum, which contains only the outer scale compensation:

$$\Phi_n(\kappa, z) = 0.033\, C_n^2(z)(\kappa^2 + \kappa_0^2)^{-11/6} \tag{3}$$

The 2D power spectrum of a thin slab of turbulence in a plane orthogonal to the direction of propagation (the z axis) is given by

$$F_\phi(\kappa_r) = 2\pi k^2\, 0.033\, (\kappa_r^2 + \kappa_0^2)^{-11/6} \int_z^{z+\Delta z} C_n^2(\xi) d\xi \tag{4}$$

where $k = 2\pi/\lambda$, Δz is the width of the turbulent slab, and $\kappa_r = (\kappa_x^2 + \kappa_y^2)^{1/2}$ (note that $\kappa_z = 0$ because we have restricted ourselves to the plane orthogonal to the z axis). This expression is simplified by using the definition of the coherence length of the turbulence

$$r_0 = 0.185 \left[\frac{\lambda^2}{\int_z^{z+\Delta z} C_n^2(\xi) d\xi} \right]^{3/5} \tag{5}$$

and the definition of $\Phi_n(\kappa, z)$ in (3) to give

$$F_\phi(\kappa_r) = 0.490 r_0^{-5/3} (\kappa_r^2 + \kappa_0^2)^{-11/6} \tag{6}$$

3 FFT-BASED PHASE SCREEN GENERATION

Now we turn our attention to the generation of phase screens which obey the statistics discussed in the previous section. It is a well known property of random processes that random realizations of a function which has a well-defined power spectrum can easily be generated by filtering a Gaussian white noise process with the square root of the spectrum, followed by an inverse Fourier transform. Thus, we can generate a (continuous) phase screen, $\phi(\vec{r})$, using

$$\phi(\vec{r}) = \int_{-\infty}^{\infty}\int h(\vec{\kappa_r}) \sqrt{F_\phi(\kappa_r)}\, e^{i\vec{r}\cdot\vec{\kappa_r}} d\vec{\kappa_r} \tag{7}$$

where $\vec{r} = (x, y)$, $h(\vec{\kappa_r})$ is a zero-mean unit-variance Hermitian complex Gaussian white noise process, and $\vec{\kappa_r} = (\kappa_x, \kappa_y \mid \kappa_z = 0)$. We must now convert (7) to a discrete formulation. We begin by approximating the integral with the summation

$$\phi(x, y) = \sum_{\kappa_x} \sum_{\kappa_y} h(\kappa_x, \kappa_y) \sqrt{F_\phi(\kappa_x, \kappa_y)}\, e^{i(\kappa_x x + \kappa_y y)} \Delta\kappa_x \Delta\kappa_y \tag{8}$$

The discrete spatial domain points x and y are given by $x = m\Delta x$ and $y = n\Delta y$, where Δx and Δy are the desired sample intervals, and m and n are integer indices. The discrete wavenumber domain sample points κ_x and κ_y are given by $\kappa_x = m'\Delta\kappa_x$ and $\kappa_y = n'\Delta\kappa_y$, where $\Delta\kappa_x$ and $\Delta\kappa_y$ are the sample intervals, and m' and n'

are integer indices. The discrete white noise process is given by

$$h(\kappa_x, \kappa_y) = \frac{g(m', n')}{\sqrt{\Delta\kappa_x \Delta\kappa_y}} \tag{9}$$

where $g(m', n')$ is a discrete Gaussian noise process defined as

$$g(m', n') = g_{real}(m', n') + i g_{imag}(m', n') \tag{10}$$

and $g_{real}(m', n')$ and $g_{imag}(m', n')$ are zero-mean Gaussian deviates with a standard deviation of $1/\sqrt{2}$. Because $h(m', n')$ is Hermitian, we require that $g(m', n') = g^*(-m', -n')$. The scaling by $\sqrt{\Delta\kappa_x \Delta\kappa_y}$ is required to make the correlation of the discrete noise process approximate a continuous 2D spatial delta function (recall a 2D spatial delta function has units of $1/\text{distance}^2$).

To implement (8) with an FFT, we convert from wavenumber space to the spatial frequency domain ($\kappa = 2\pi f$) and make the following definitions. The x and y sizes of the screen are G_x and G_y, each with N_x and N_y points, respectively (N_x and N_y are both powers of two, as required by the FFT). The corresponding sample intervals are $\Delta x = G_x/N_x$ and $\Delta y = G_y/N_y$. The spatial frequencies, f_x and f_y, are defined by $f_x = m'\Delta f_x$ and $f_y = n'\Delta f_y$, where $\Delta f_x = 1/G_x$ and $\Delta f_y = 1/G_y$. Substituting the expression given in (6) for F_ϕ and using a little algebra, we arrive at the following expression for a phase screen:

$$\phi(m, n) = \sum_{m'=-N_x/2}^{N_x/2-1} \sum_{n'=-N_y/2}^{N_y/2-1} h(m', n')\, f(m', n')\, e^{i2\pi\left(\frac{m'm}{N_x} + \frac{n'n}{N_y}\right)} \tag{11}$$

where

$$f(m', n') = \frac{2\pi}{\sqrt{G_x G_y}} \sqrt{0.00058}\, r_0^{-5/6} (f_x^2 + f_y^2)^{-11/12} \tag{12}$$

is the turbulence spatial filter and $h(m', n')$ is the white noise process (note that the scaling shown in (9) and the multiplication by the sample intervals in (8) have been incorporated into the filter function). The origin of the filter function, which determines the average phase delay of the screen, is set to zero. The average phase delay has no effect on the speckle image formation process; hence, it is acceptable to set it to zero. Equation (11) is now in a form easily implemented using an FFT, and we see that the phase screen $\phi(m, n)$ is simply the inverse FFT of the product of the filter function $f(m', n')$ and a white noise realization of $h(m', n')$.

A sample phase screen generated by this method is shown in figure 1a. The size of the screen is 2 m by 2 m, 256 by 256 sample points, r_0 is 0.1 m, and the outer scale, L_0, is 10 m. Notice that the screen is periodic at the edges and hence, the overall tilt of the screen is zero. The speckle image corresponding to this phase screen is shown in figure 1b, where a 1 m circular aperture was used to create the image.

4 EVALUATING THE ACCURACY OF THE SIMULATION

The question then arises, how accurate is the phase screen we just produced? Typically, phase screens are evaluated by how well they reproduce the desired phase structure function for the given turbulence model. The phase structure function is defined as

$$D_\phi(\vec{r}) = \langle (\phi(\vec{\rho} + \vec{r}) - \phi(\vec{\rho}))^2 \rangle \tag{13}$$

which represents the average squared difference of the phase of the screen for pairs of points of varying location and separation. The structure function is related to the 2D autocorrelation of the phase screen, which is defined as

$$B_\phi(\vec{r}) = \langle \phi(\vec{\rho} + \vec{r}) \phi(\vec{\rho}) \rangle \tag{14}$$

and is related to the structure function via

$$D_\phi(\vec{r}) = 2(B_\phi(0) - B_\phi(\vec{r})) \tag{15}$$

The 2D autocorrelation function is also related to the 2D power spectrum defined earlier:

$$B_\phi(\vec{r}) = \int_{-\infty}^{\infty}\int F_\phi(\vec{\kappa_r})e^{i\vec{r}\cdot\vec{\kappa_r}}d\vec{\kappa_r} \tag{16}$$

For the Kolmogorov turbulence statistics discussed earlier, the phase structure function has been shown to have the following forms:

$$D_\phi(r) = 6.88(r/r_0)^{5/3} \tag{17}$$

for the case of an infinite outer scale ($\kappa_0 \to \infty$), and

$$D_\phi(r) = 6.16r_0^{5/3}\left[\frac{3}{5}\left(\frac{L_0}{2\pi}\right)^{5/3} - \frac{\left(\frac{rL_0}{4\pi}\right)^{5/6}}{\Gamma(11/6)}K_{5/6}\left(\frac{2\pi r}{L_0}\right)\right] \tag{18}$$

for the case of a finite outer scale [6], where $K_{5/6}(-)$ is a modified Bessel function of the third kind, and $\Gamma(-)$ is the gamma function.

Many authors evaluate the accuracy of their simulations by using an ensemble of random phase screens over which to compute the average phase structure function. It is, perhaps, more insightful to compute the expected value of the structure function (we will refer to this as the expected structure function), which can be done deterministically. Structure functions computed over an ensemble of random phase screens will, given a statistically large enough sample set of screens, converge to this expected structure function. The expected structure function is computed by taking the inverse FFT of the 2D power spectrum, $F_\phi(\kappa_r)$, to get the 2D autocorrelation (this is a numerical implementation of (16)), and then applying (15). Note that there should be no numerical problems with this because the pole at the origin of the power spectrum has been set to zero. The 2D autocorrelation function for the FFT-based phase screen is given by

$$B_\phi(m,n) = \sum_{m'=-N_x/2}^{N_x/2-1}\sum_{n'=-N_y/2}^{N_y/2-1} f^2(m',n')\, e^{i2\pi\left(\frac{m'm}{N_x}+\frac{n'n}{N_y}\right)} \tag{19}$$

where $f(m',n')$ is the filter function defined in (12). The expected structure function is then computed from (15). An example of an expected structure function for the FFT-based simulation is shown in figure 2, along with the theoretical structure function for the simulation parameters described earlier. The expected structure function is well below that predicted by theory. The difference occurs because the FFT-based simulation method does not adequately sample the low frequency content of the 2D power spectrum, which we discuss next.

5 LIMITATIONS OF THE FFT-BASED SIMULATOR

Although the FFT-based simulation method is simple to implement, it has inherent limitations. The minimum and maximum spatial frequencies of the screens generated by this method are $f_{min} = \Delta f = 1/G$ and $f_{max} = N\Delta f/2 = 1/(2\Delta x)$, where G is the size of the screen, N is the number of points, and Δx is the sample interval ($\Delta x = G/N$). For a typical 256 by 256 screen of size 2 m (0.0078125 m sampling), we have $f_{min} = 0.5$ m^{-1} and $f_{max} = 64$ m^{-1}. These correspond to maximum and minimum representable scale sizes of 2 m and 0.015625 m, respectively. Typically, the scale sizes of turbulent eddies vary from an outer scale of tens of meters down to an inner scale of just a few millimeters, neither of which extreme is sampled properly in the FFT-based simulation method.

The improper sampling of the inner scale is not critical, as discussed earlier, because of the large attenuation of $\Phi_n(\kappa_i, z)$ relative to $\Phi_n(\kappa_0, z)$. Indeed, it is the outer scale which is the main contributor to the low frequency characteristics of the turbulence, especially tilt. Hence, adequate sampling of the outer scale portion of the power spectrum is required to accurately simulate large-scale turbulence characteristics. Figure 3 shows a 1D section of the spectrum near the origin which emphasizes this point (the parameters are the same as those of the earlier examples). The outer scale occurs at 0.1 m^{-1} and the first sample point in the spectrum occurs at 0.5 m^{-1}.

Clearly, a major portion of the spectral energy near the origin is not sampled properly. Therefore, the tilt and other manifestations of the large-scale turbulence characteristics will not be correct for this screen. In an attempt to sample more of the low frequency portion of the spectrum, we can increase the size of the grid while maintaining the same sample interval; however, the sheer size of the screen soon becomes a problem. If we use a screen that is five times the size of the outer scale, as reference [6] suggests is sufficient to properly sample the outer scale, then a 50 m grid is required for a 10 m outer scale. Using the same sample intervals as in the above examples, this would require an 8192 by 8192 point screen, which is clearly not practicable.

There are a couple of methods currently in use to compensate for this problem. One is to generate very large screens and extract a small center portion; the idea being that the low frequency characteristics will be accurate over a small portion of the large screen. Another is to add low order Zernike modes using Noll's statistics [10]. Both of these methods require using large rectangular or square screens, which is not practical when very long narrow screens are desired.

6 ADDITION OF LOW FREQUENCY INFORMATION USING SUBHARMONICS

Recently, several researchers have begun using subharmonics to help solve this problem. A subharmonic is a sinusoid with a period larger than the screen size (possibly many times larger than the screen size) which has a spatial frequency lower than the lowest possible representable frequency of the screen. By sampling the low frequency subharmonic portion of the spectrum and incorporating that information into the FFT-based phase screen, we should be able to generate phase screens which accurately model Kolmogorov turbulence at large scale sizes.

6.1 The subharmonic method of Herman and Strugala

In reference [6], Herman and Strugala incorporate subharmonic information by generating the power spectrum of a low frequency phase screen which is many times larger than than the high frequency screen of the FFT-based method. The sample interval they choose for the large screen is the length of the original FFT-based screen so that the high frequency screen fits precisely in the rectangle formed by four adjacent samples of the low frequency screen. The square root of the low frequency power spectrum is multiplied by white noise and then Fourier inverted; however, the resulting low frequency screen is sampled only at the finely spaced sample points of the high frequency screen. This sampling of the low frequency screen is essentially a form of interpolation and is accomplished by brute-force evaluation of the Fourier kernel at the high frequency screen points. The high frequency screen and the interpolated low frequency screen are then added to produce the final phase screen.

If N_x' and N_y' are the number of points in the x and y directions of the low frequency grid, then the low frequency screen evaluated on the high frequency screen grid is given by

$$\phi_{LF}(m,n) = \sum_{m'=-N_x'/2}^{N_x'/2-1} \sum_{n'=-N_y'/2}^{N_y'/2-1} h(m',n')\ \tilde{f}(m',n')\ e^{i2\pi\left(\frac{m'm}{N_x'N_x}+\frac{n'n}{N_y'N_y}\right)} \tag{20}$$

where

$$\tilde{f}(m',n') = \frac{2\pi}{\sqrt{N_x'G_xN_y'G_y}}\sqrt{0.00058}\ r_0^{-5/6}(f_x^2+f_y^2)^{-11/12} \tag{21}$$

is the low frequency turbulence filter function, $h(m',n')$ is the white noise process, and f_x and f_y are the spatial frequencies, defined by $f_x = m'/(N_x'G_x)$ and $f_y = n'/(N_y'G_y)$. The filter function is denoted with a tilde to indicate that it has been scaled by $1/2$ at the endpoints ($1/4$ at the corners) $m' = \pm N_x'/2$ and $n' = \pm N_y'/2$. This is to account for the fact that the patches of area corresponding to the endpoints of the subharmonic portion of the spectrum overlap the patches of area corresponding to the first sample points of the high frequency portion of the spectrum. Also, the filter function is set to zero at the origin, as previously discussed. The relationship between the high and low frequency spectra is shown in figure 4. We see that the area patch representing the origin in the high frequency spectrum has been replaced by the finely-spaced grid of small subharmonic patches (the sample point at the origin is still zero). The final phase screen is generated by summing $\phi(m,n)$ and $\phi_{LF}(m,n)$.

The expected structure function for this method of phase screen generation is derived by summing the 2D

autocorrelations of the high and low frequency screens to form an overall autocorrelation, and then applying (15). The autocorrelation for the low frequency screen is given by

$$B_{\phi_{LF}}(m,n) = \sum_{m'=-N_x'/2}^{N_x'/2-1} \sum_{n'=-N_y'/2}^{N_y'/2-1} \tilde{f}^2(m',n')\, e^{i2\pi\left(\frac{m'm}{N_x'N_x}+\frac{n'n}{N_y'N_y}\right)} \tag{22}$$

where $\tilde{f}(m',n')$ is the filter function (scaled at the endpoints of the summation) defined in (21).

Examples of the expected structure functions for this subharmonic method using various low frequency grid sizes are shown in figures 5 and 6. For a 10 m outer scale (figure 5), we see that the expected structure function gets closer to the theoretical structure function as more low frequency grid points are used. However, there is no further improvement for grid sizes larger than 16 by 16, and a significant discrepancy still exists. The results are similar for the case of an infinite outer scale (figure 6), but the discrepancy is even larger (the maximum grid size used is 64 by 64, for computational reasons). Evidently, the low frequency portion of the spectrum is still not sampled finely enough to give a structure function which closely matches the theoretical one.

6.2 The subharmonic method of Lane, Glindemann, and Dainty

In reference [2], Lane, Glindemann, and Dainty present another method of incorporating subharmonic information. They divide up the area patch of the origin of the high frequency spectrum into nine equally sized sub-patches, each with 1/9 of the area of the original patch size. Sample points are placed in the eight outer sub-patches, creating a subharmonic grid similar to that of Herman and Strugala. However, the process is now repeated using the remaining small patch at the origin, creating multiple subharmonic levels or sets. The sample sizes of the patches at the pth subharmonic level ($p \geq 1$) are then given by $\Delta\kappa_{x_p} = \Delta\kappa_x/3^p$ and $\Delta\kappa_{y_p} = \Delta\kappa_y/3^p$. The relationship between the high and low frequency spectra is illustrated in figure 7.

The method of incorporating the subharmonic information onto the high frequency grid described in [2] is different from that described in section 6.1. It uses shifted sinc functions to resample the subharmonic data onto the high frequency spectrum, and generates the final phase screen with an inverse FFT. Gibb's phenomenon ringing occurs in the screen, so screens twice the desired size must be generated and the desired size portion extracted from the center of the screen. This is not practical when very long narrow screens are desired, so we have modified the algorithm to use the same method of incorporating the subharmonic information as described in section 6.1. The modified algorithm should still give a good representation of the ability of the original algorithm to reproduce correct low frequency turbulence characteristics, because the same spectral information is being used. Therefore, assuming N_p subharmonic levels, the low frequency screen using the modified algorithm of Lane, et al. is given by

$$\phi_{LF}(m,n) = \sum_{p=1}^{N_p} \sum_{m'=-1}^{1} \sum_{n'=-1}^{1} h(m',n')\, f(m',n')\, e^{i2\pi 3^{-p}\left(\frac{m'm}{N_x}+\frac{n'n}{N_y}\right)} \tag{23}$$

where

$$f(m',n') = \frac{2\pi 3^{-p}}{\sqrt{G_x G_y}} \sqrt{0.00058}\, r_0^{-5/6} (f_x^2 + f_y^2)^{-11/12} \tag{24}$$

is the low frequency turbulence filter function, $h(m',n')$ is the white noise process, and f_x and f_y are the spatial frequencies, defined by $f_x = 3^{-p} m' \Delta f_x$ and $f_y = 3^{-p} n' \Delta f_y$. The remaining parameters are the same as those defined in section 3. The filter function is set to zero at the origin, as previously discussed; however, there is no scaling of the spectrum at the endpoints of the summation, since there is no overlapping of area patches between the high and low frequency spectra.

The expected structure function is computed using the same method discussed in section 6.1. The autocorrelation function to be used in the calculation of the expected structure function for this subharmonic method is given by

$$B_\phi(m,n) = \sum_{p=1}^{N_p} \sum_{m'=-1}^{1} \sum_{n'=-1}^{1} f^2(m',n') e^{i2\pi 3^{-p}\left(\frac{m'm}{N_x}+\frac{n'n}{N_y}\right)} \tag{25}$$

where $f(m', n')$ is the filter function defined in (24).

Examples of the expected structure functions for this subharmonic method are shown in figures 8 and 9 for various numbers of subharmonic levels. The examples correspond to the same simulation parameters used to test the subharmonic method of Herman and Strugala. For the case of the 10 m outer scale, shown in figure 8, the structure function approaches the theoretical structure function rapidly with the addition of just two subharmonic levels. However, adding more subharmonic levels yields no further improvement in the structure function. The method also shows rapid improvement in the infinite outer scale case, shown in figure 9. There is only slight improvement from 10 to 15 subharmonic levels, and there is still a discrepancy between the expected structure function and the theoretical. After 15 levels of subharmonics (in the case of the infinite outer scale), numerical problems begin to occur. Each subsequent subharmonic level samples the spectrum closer and closer to the pole at the origin, which eventually causes dynamic range problems for the floating point numbers in the simulation, even when using double precision arithmetic. Although the subharmonic method of Lane et al. yields a structure function which approximates theory, there is still a discrepancy, especially at large separations. Again, it appears as though the low frequency portion of the spectrum is still not sampled properly.

7 A NEW SUBHARMONIC METHOD

We have developed a new subharmonic method, which is a hybrid of the two previous techniques, to correct this problem. Our method uses a modified version of the subharmonic level concept of Lane et al. and the direct Fourier inversion technique of Herman and Strugala. We begin by increasing the size of the origin patch by a factor of two in each direction (an increase in area of four). This causes the origin patch to overlap the first samples of the high frequency spectrum. Hence, we scale the overlapped points of the high frequency spectrum to compensate. The points at indices $(\pm 1, 0)$ and $(0, \pm 1)$ are scaled by 1/2, whereas the points at indices $(\pm 1, \pm 1)$ are scaled by 3/4. The large origin patch is then divided into nine sub-patches, as in the method of Lane et al. Instead of placing sample points in the eight outer sub-patches, we now subdivide each sub-patch into 4 smaller sub-patches, placing a sample point in each. Thus, we have 32 sample points in each subharmonic level. We continue to add further subharmonic levels, as before. The relationship between the high and low frequency spectra is shown in figure 10.

Again, assuming N_p subharmonic levels, the low frequency screen for this method is given by

$$\phi_{LF}(m,n) = \sum_{p=1}^{N_p} \sum_{m'=-3}^{2} \sum_{n'=-3}^{2} h(m',n')\, f(m',n')\, e^{i2\pi 3^{-p}\left(\frac{(m'+0.5)m}{N_x} + \frac{(n'+0.5)n}{N_y}\right)} \tag{26}$$

where

$$f(m',n') = \frac{2\pi 3^{-p}}{\sqrt{G_x G_y}} \sqrt{0.00058}\, r_0^{-5/6} (f_x^2 + f_y^2)^{-11/12} \tag{27}$$

is the low frequency turbulence filter function, $h(m', n')$ is the white noise process, and f_x and f_y are the spatial frequencies, defined by $f_x = 3^{-p}(m' + 0.5)\Delta f_x$ and $f_y = 3^{-p}(n' + 0.5)\Delta f_y$. The remaining parameters are the same as those defined in section 3. The filter function is set to zero at the origin, as previously discussed. Also, the scaling to compensate for the overlapping regions takes place in the high frequency spectrum (i.e., not in the filter function), as noted above.

The expected structure function is computed using the same method discussed in section 6.1. The autocorrelation function to be used in the calculation of the expected structure function for our new subharmonic method is given by

$$B_\phi(m,n) = \sum_{p=1}^{N_p} \sum_{m'=-3}^{2} \sum_{n'=-3}^{2} f^2(m',n') e^{i2\pi 3^{-p}\left(\frac{(m'+0.5)m}{N_x} + \frac{(n'+0.5)n}{N_y}\right)} \tag{28}$$

where $f(m', n')$ is the filter function defined in (27).

Examples of the expected structure functions are shown in figures 11 and 12 for various numbers of subharmonic levels. The examples correspond to the same simulation parameters used previously. In the case of the 10 m outer scale, shown in figure 11, the structure function comes extremely close to the theoretical structure function

with the addition of just two subharmonic levels. Adding more subharmonic levels yields no further improvement, which leads us to believe that there is still some slight improper sampling occurring; however, the result is quite good. This method also shows excellent results for the case of the infinite outer scale, which is shown in figure 12. Here again, we can only achieve 15 subharmonic levels because of numerical problems, but the results for 10 and 15 levels are quite good compared to theory. Hence, we see that the increased sampling density has resulted in structure functions which are very close to those predicted by theory. We can now use this method to create very long and narrow screens to be used in time varying simulations.

8 CONCLUSIONS

We have developed a new method of phase screen generation which is well suited to the problem of generating very long narrow screens for time dependent turbulence simulation studies. There are no edge effects in the screens generated by this method – there is no ringing, and no phase wrap at the edges. The structure functions for this new method match very closely the structure functions of Kolmogorov turbulence theory. The spatial correlation statistics need to be studied further and compared to the theory presented in [11].

9 ACKNOWLEDGEMENTS

We would like to thank Claire Max, Jim Brase, and all the members of the LLNL Laser Guide Star project for their support of this work.

This work was performed under the auspices of the U. S. Department of Energy by the Lawrence Livermore National Laboratory under contract number W-7405-ENG-48.

10 REFERENCES

[1] N. Roddier, "Atmospheric wavefront simulation and Zernike polynomials," *SPIE* Vol. 1237, 668–679 (1990).

[2] R. G. Lane, A. Glindemann, and J. C. Dainty, "Simulation of a Kolmogorov phase screen," in *Waves in Random Media*, Vol. 2, No. 3, 209–224 (1992).

[3] B. L. McGlamery, "Computer simulation studies of compensation of turbulence degraded images," *SPIE* Vol. 74, 225–233, (1976).

[4] J. M. Martin and S. M. Flatte, "Intensity images and statistics from numerical simulation of wave propagation in 3-D random media," *JOSA A* Vol. 27, No. 11, 2111–2126 (1988).

[5] E. M. Johansson, T. W. Lawrence, J. P. Fitch, and R. J. Sherwood, "Simulating speckle interferometry," *SPIE* Vol. 1237, 448-458 (1990).

[6] B. J. Herman and L. A. Strugala, "Method for inclusion of low-frequency contributions in numerical representation of atmospheric turbulence," *SPIE* Vol. 1221, 183–192 (1990).

[7] J. W. Goodman, *Statistical Optics*, Wiley, New York, 1985.

[8] D. M. Goodman, T. W. Lawrence, E. M. Johansson, and J. P. Fitch, "Bispectral speckle interferometry to reconstruct extended objects from turbulence-degraded telescope images," in *Handbook of Statistics, Vol. 10*, North Holland, Amsterdam, 1993.

[9] R. R. Parenti, "Construction of phase screens for turbulence models," MIT Lincoln Laboratory Memorandum No. 54-PM-PBP-002, June 1, 1992.

[10] R. J. Noll, "Zernike polynomials and atmospheric turbulence," *JOSA* Vol. 66, No. 3, 207–211 (1976).

[11] G. C. Valley and S. M. Wandzura, "Spatial correlation of phase-expansion coefficients for propagation through atmospheric turbulence," *JOSA* Vol. 69, No. 5, 712–717 (1979).

This work was performed under the auspices of the Department of Energy by the Lawrence Livermore National Laboratory under contract W-7405-Eng-48.

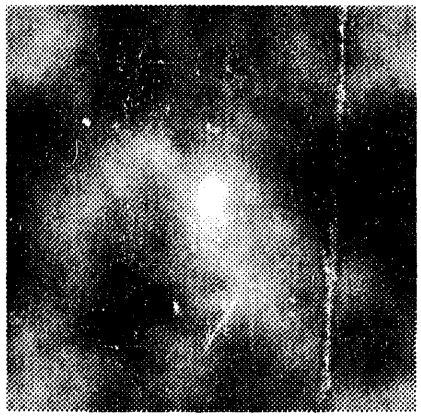

a. Phase screen

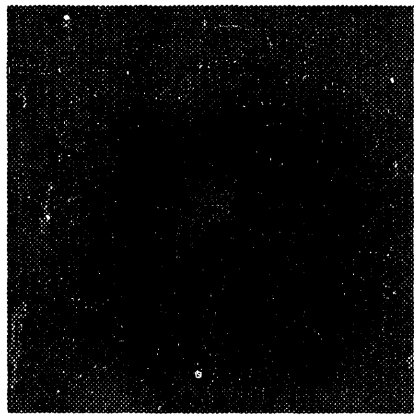

b. Speckle image

Figure 1. a) A sample phase screen using the FFT-based simulator. The screen is of size 2 m by 2 m, 256 by 256 points, $r_0 = 0.1$ m, and $L_0 = 10$ m. b) The speckle image generated using the screen of part a, assuming a 1 m circular aperture.

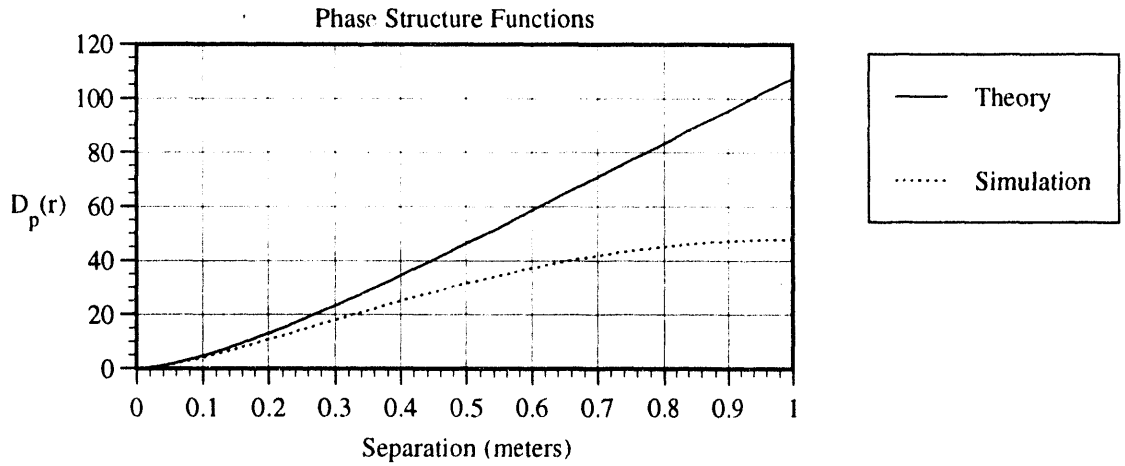

Figure 2. The expected structure function for the phase screen of figure 1a along with the theoretical structure function.

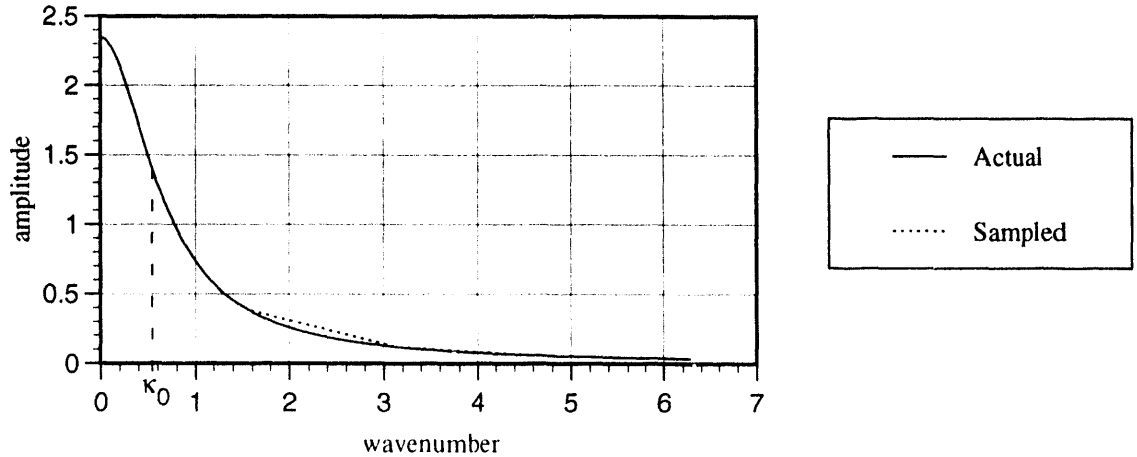

Figure 3. A 1D slice of the spectrum used to generate the phase screen of figure 1a. The first sample point of the spectrum is at $0.5 m^{-1}$ and the outer scale is located at $0.1 m^{-1}$. Most of the low frequency energy at the origin is not sampled by this method of simulation.

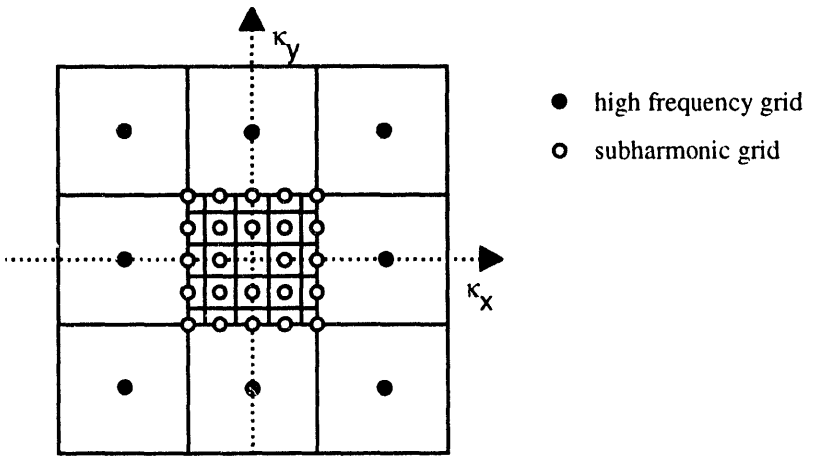

Figure 4. The relationship between the high and low frequency spectra in the subharmonic method of Herman and Strugala

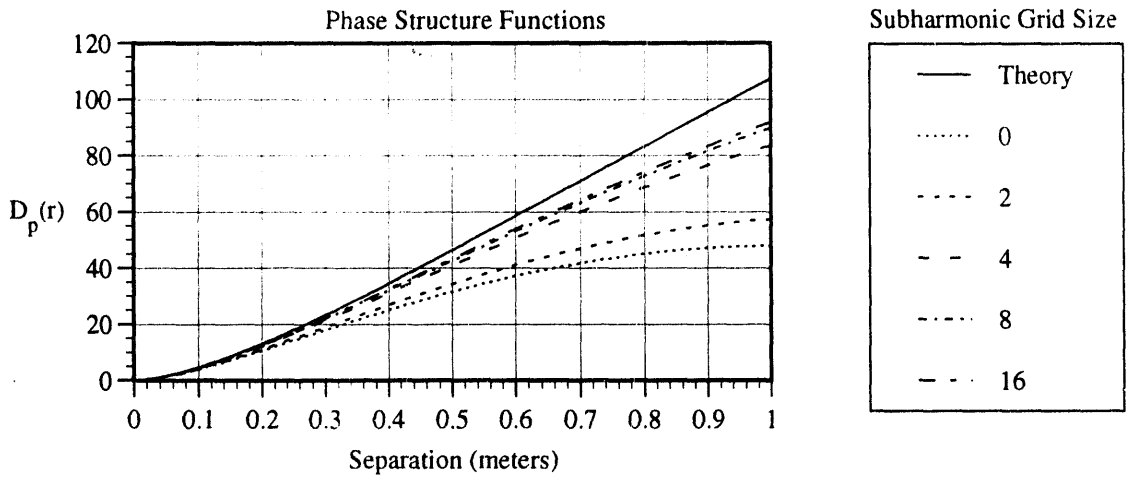

Figure 5. A comparison with theory of structure functions for the subharmonic method of Herman and Strugala using various subharmonic grid sizes, for a 10 m outer scale.

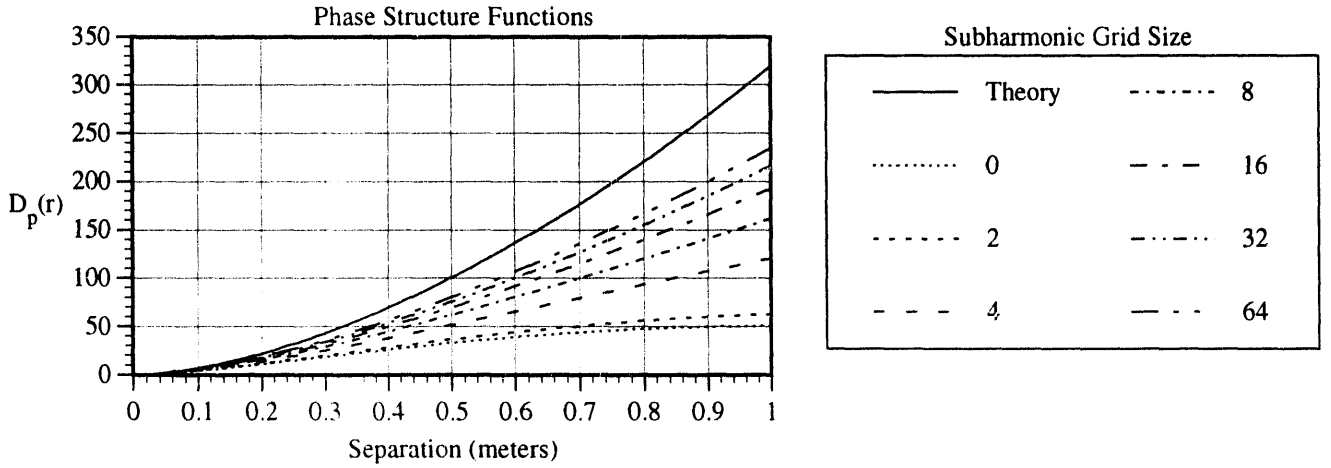

Figure 6. A comparison with theory of structure functions for the subharmonic method of Herman and Strugala using various subharmonic grid sizes, for an infinite outer scale.

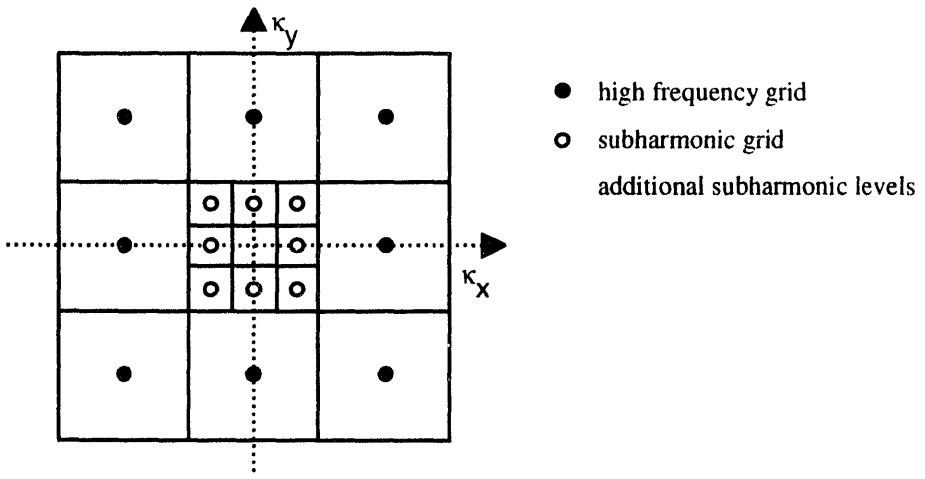

Figure 7. The relationship between the high and low frequency spectra in the subharmonic method of Lane et al.

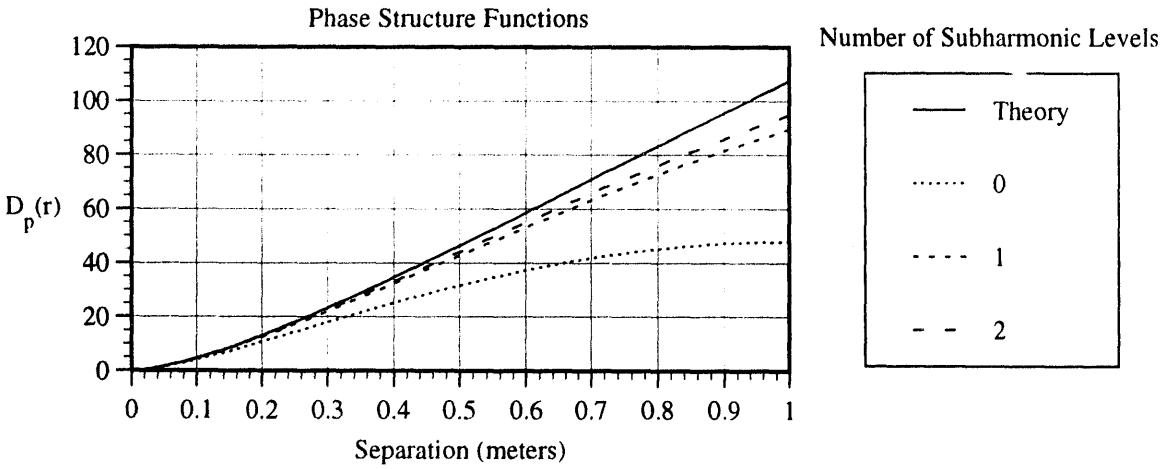

Figure 8. A comparison with theory of structure functions for the subharmonic method of Lane et al. using various numbers of subharmonic levels, for a 10 m outer scale.

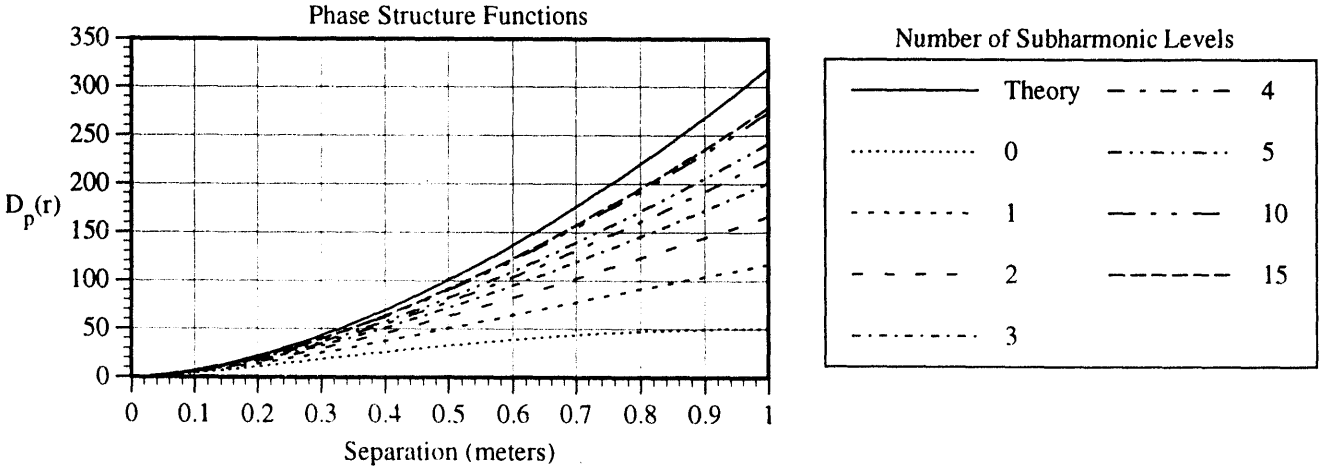

Figure 9. A comparison with theory of structure functions for the subharmonic method of Lane et al. using various numbers of subharmonic levels, for an infinite outer scale.

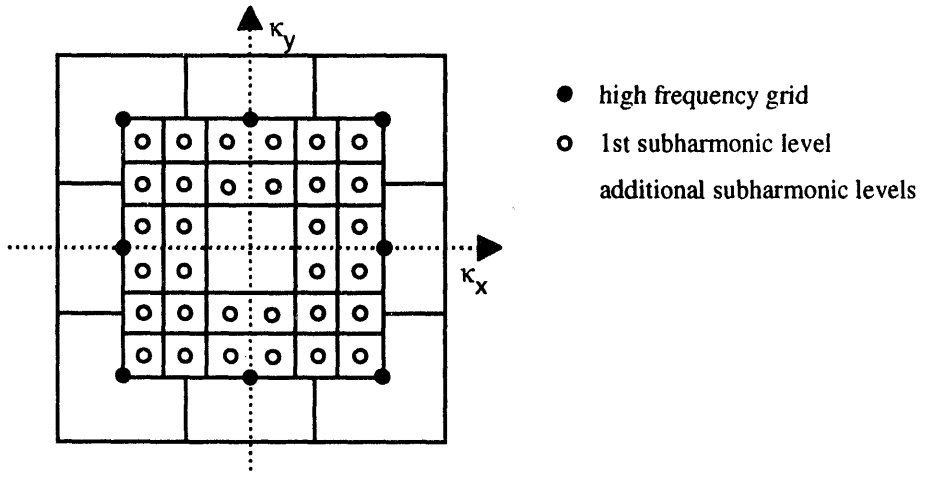

Figure 10. The relationship between the high and low frequency spectra in the new hybrid subharmonic method.

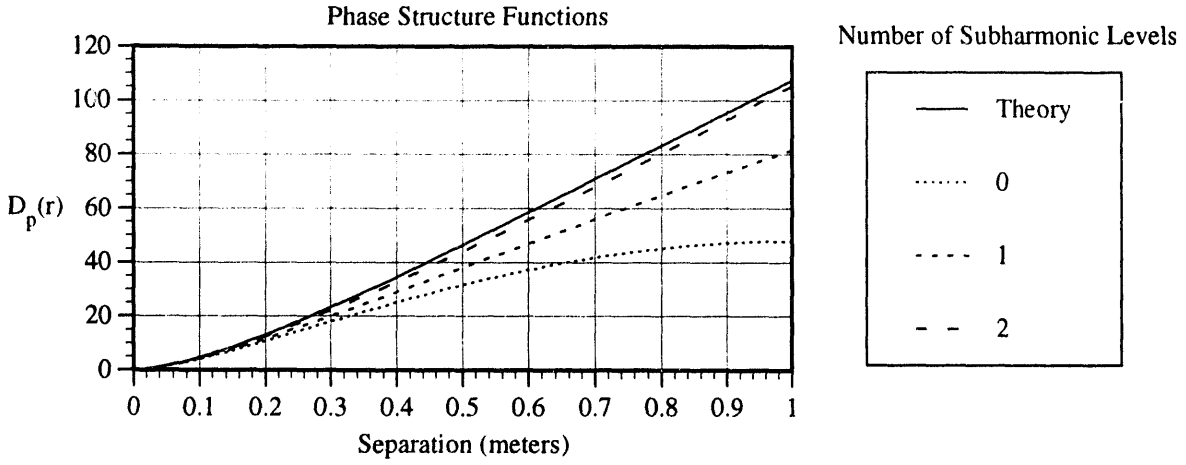

Figure 11. A comparison with theory of structure functions for the new hybrid subharmonic method using various numbers of subharmonic levels, for a 10 m outer scale.

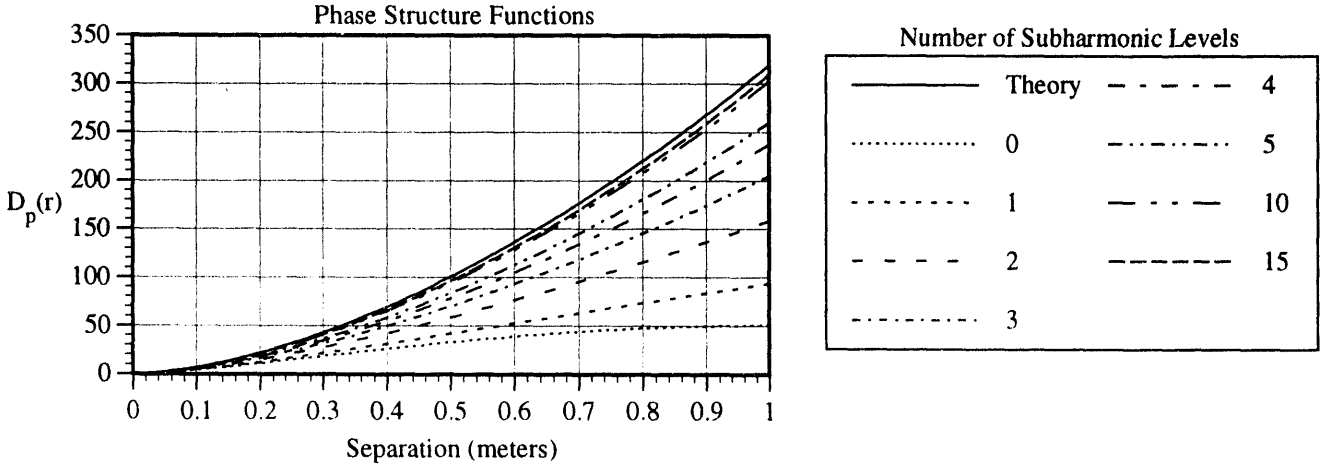

Figure 12. A comparison with theory of structure functions for the new hybrid subharmonic method using various numbers of subharmonic levels, for an infinite outer scale.

DATE
FILMED
9/26/94

END